EPJ Photovoltaics **14**, 14 (2023)

https://doi.org/10.1051/epjpv/2023002

Special Issue on 'WCPEC-8: State of the Art and Developments in Photovoltaics', edited by Alessandra Scognamiglio, Robert Kenny, Shuzi Hayase and Arno Smets

Available online at: www.epj-pv.org

REGULAR ARTICLE

OPEN ACCESS

Evaluating the effects of photovoltaic module heating during electroluminescence inspection

Lukas Koester[1,2,*], Emanuel Vallarella[3], Atse Louwen[1], Sascha Lindig[1], and David Moser[1]

[1] Institute for Renewable Energy, EURAC Research, Viale Druso 1, Bolzano 39100, Italy
[2] Dipartimento di Energia, Politecnico di Milano, Via Lambruschini 4, 20156 Milano, MI, Italy
[3] Huawei Nuremberg Research Center, Power Conversion Technology Laboratory, Nürnberg, Germany

Received: 14 July 2022 / Received in final form: 18 October 2022 / Accepted: 9 January 2023

Abstract. The application of electroluminescence imaging of photovoltaic modules increased in the last years, due to the reliable and detailed identification of degradation and failures. In future plants the time-consuming connection of power supplies could be overcome by use of inverters with bi-directional functionality, allowing backpowering of connected module strings directly. Temperature influences the open-circuit voltage of photovoltaic modules and must therefore be considered during backpowering. This work investigates the heating due to backpowering of photovoltaic modules of different types during electroluminescence inspection. The temperature increase until saturation is estimated by energy balance calculations and experimentally verified to be around 20 °C, with resulting voltage drops of up to 3 V. Further, these changes have an effect on the recorded luminescence intensity: a decrease of the electroluminescence signal intensity between beginning of backpowering and reaching saturation temperature is shown. For application of the results to a real-world scenario, the electroluminescence window of an electroluminescence-ready inverter is introduced, giving the boundaries of current and voltage that can be supplied. Combined with a simulation of the dark current–voltage curves of a connected photovoltaic module string, the electroluminescence inspection possibilities are visualized. Finally, the applicability of this heating phenomenon for snow melting is discussed.

Keywords: PV inspection / operation and maintenance / electroluminescence / snow melting

1 Introduction

Numerous methods are available to inspect photovoltaic (PV) power plants during their operational phase, one of which is electroluminescence (EL) inspection. EL works through forward biasing the PV solar cells p-n junctions by injecting a forward current into the module [1], commonly described under the synonym backpowering. This triggers recombination processes with emission of luminescence radiation from the solar cells [2]. The luminescence signal is small compared to sun irradiation, hence EL inspection is commonly performed during the night, although daylight EL inspection is possible as well [3]. The use of EL in the field increased strongly in the last years due to improvements in the technique allowing for reliable and detailed identification of degradation and failures, and the development towards faster imaging and therefore decreased costs. While the technical specification (TS) by the international electrotechnical commission (IEC) 60904-13 [1] describes EL inspections of single PV modules in laboratory conditions, a new TS is currently under preparation which will deal with EL measurements of online PV strings in utility scale plants [4]. From a financial point of view, the speed of EL inspections in large scale PV plants is crucial. A key factor impacting the speed is the procedure of applying the necessary power to the PV modules. Commercially available power supplies can supply sufficient power to forward-bias up to single strings of PV modules, while prototypes exits that are able to perform automated switching between up to 100 strings, which allows unmanned aerial vehicle (UAV) mounted inspections of PV plant sections of up to 500 kWp, without moving the power supply [5]. Nevertheless, the extra hardware requires installation and reconfiguration of the cabling before every EL inspection. In future plants the time-consuming installation part of power supplies could be overcome by using inverters with bi-directional functionality, allowing backpowering of connected module strings directly. Nowadays, existing inverters can be upgraded to perform backpowering for EL [6].

During EL inspection, the cell temperature is increased due to the supplied current. This results in a decrease of the cells' open-circuit voltage (V_{OC}). Although the shift in V_{OC}

* e-mail: lukas.koester@eurac.edu

is small in one module, it might be non-negligible if a whole PV module string is considered. Especially in the case for EL-ready inverters, these considerations need to be taken into account in the planning phase of a PV plant already. Thus, to identify reliably the best conditions for EL imaging on large PV strings, the heating process must be understood and considered fully. The heating process is described well for PV modules during normal operation under sun irradiation [7–11], but not when the power is supplied directly to the module string during backpowering. Instead, hot-spot formation describes the heating of solar cells in reverse bias [12,13]. Another factor is the stability of the recorded EL signal: The intensity of luminescence radiation depends exponentially on temperature and voltage. A cell temperature increase will result in a reduction of luminescence signal intensity [14,15]. Although a small effect, it needs to be investigated and quantified for future EL inspections.

A power supply unit (PSU), such as standard power supplies or EL-ready inverters, comes with a specific operational range, usually defined by voltage range and a maximum current. The latest TS for EL defines the amount of current to feed into a PV module for reliable EL inspection (i.e. I_{SC} and $0.1 \times I_{SC}$) [1]. The TS recommends to have a power supply with sufficient voltage to provide I_{SC}, which should be at V_{OC} level, but can be significantly higher [1]. Considering that these currents are necessary for proper EL inspection and the specific operational range of PSUs, it minimizes the range of how many modules are allowed per string.

To address these questions, the temperature increase of PV modules during EL inspection is investigated from a physics-based point of view. For an understanding of the processes, the investigation is approached for single modules of different technologies. These results are then discussed in the context of PV module strings. First, the saturation temperature during backpowering is derived by energy balance calculations and then examined through experimental temperature measurements during EL backpowering. Continuous EL imaging allows to investigate the impact heating has on the EL signal intensity. Simulations of the dark current–voltage (I–V) curves of different temperatures of a PV string compared to the voltage and current boundaries of an EL-ready inverter are performed, to identify an EL window with the necessary conditions to perform EL inspections. Finally, the applicability of the heating effect for snow melting is discussed.

This work builds up as follows: Section 2 describes the theoretical calculation of the maximum temperature and introduces the theory behind the luminescence intensity. Further, the experimental setup and the simulation principle of dark I–V curves are described. In Section 3, the results of calculations, experiments and simulation are shown. These results are then discussed in Section 4, where as well the usage of the EL window and the applicability of heating for snow melting is discussed. Finally, Section 5 summarizes the work and gives an outlook on the future of EL inspections. A summarized version of this work was presented at the *8th World Conference on Photovoltaic Energy Conversion* [16].

2 Methods

2.1 Theoretical background

The process of PV module heating under normal operation conditions is well known. It depends mainly on environmental conditions like solar irradiance, ambient temperature and wind speed [17]. While heating is mainly caused by the sun's irradiation, the ambient temperature and wind have usually a cooling effect. The cell temperature affects V_{OC} and I_{SC}, so that an increase in PV module temperature results in reduced maximum power [17], typically around 0.3–0.4%/K depending on the PV module technology. Therefore, PV module data sheets usually provide the temperature coefficients for short circuit current, open circuit voltage and maximum power (α_{Isc}, β_{Voc} and γ_{Pm}, respectively).

The heating process during EL inspection instead is independent of the solar irradiance, as performed by night (daylight EL is not considered here). Therefore, heating depends on the supplied power P_{in}, while ambient temperature and wind speed, considered constant, force the module to maintain its original temperature, resulting in a cooling effect. Equilibrium is reached with the PV module at saturation temperature T_{sat}. In forward bias, a forward current injects carriers in the solar cell. The series resistance of the solar cell layers and the p-n junction lead to dissipation of the supplied power and therefore heating of the solar cells [18]. Further, the excess minority carrier density is increased, resulting in enhanced recombination, including radiative recombination and photon emission [19]. These photons, emitted in the near infrared regime, are the luminescence signal, and can be captured by an Indium Gallium Arsenide (InGaAs) camera for EL imaging. The amount of photons emitted by the solar cell is given by the EL signal intensity Φ_{EL}, which is correlated to the cell voltage V and temperature T by [14]

$$\Phi_{EL} = EQE \cdot \Phi_{BB} \left(\exp \frac{qV}{k_B T} - 1 \right) \tag{1}$$

which further depends on the external photovoltaic quantum efficiency EQE, the black body radiation Φ_{BB}, the elementary charge q and Boltzmann constant k_B. For the present investigation, the impact of voltage and temperature will be of interest.

2.2 PV modules under investigation

For the experimental part of our investigation of the heating effect, three common PV module types are selected: a bifacial module with hetero junction technology (HJT) cells, and two monofacial modules with mono-crystalline Silicon (c-Si) cells: one with passivated emitter and rear contact (PERC) and the other with interdigitated back contact (IBC) technology. These chosen PV module technologies represent the majority of PV modules being installed now and to be expected in the next decade [20]. The electrical parameters of the selected modules are given in Table 1.

Table 1. Data sheet electrical parameters of photovoltaic modules under investigation.

Variable	Unit	HJT	PERC	IBC
Bifacial	–	Yes	No	No
P_{nom}	W	360	310	330
V_{OC}	V	52.6	39.8	64.9
I_{SC}	A	8.9	9.7	6.5
V_{MP}	V	42.8	33.8	54.7
I_{MP}	A	8.4	9.2	6.0
$\alpha_{I_{\mathrm{sc}}}$	%/°C	0.014	0.04	0.05
$\beta_{V_{\mathrm{oc}}}$	%/°C	–0.285	–0.31	–0.26
γ_{Pm}	%/°C	–0.327	–0.40	–0.33
N_{cell}	–	72	60	96
A_{cell}	cm^2	243.7	243.7	145.6
V_{OC}/cell	V	0.73	0.66	0.68

2.3 Energy balance principle

The calculation of balance between fed and emitted energy allows to estimate the final cell temperature. The fed energy is given by the supplied power $P_{\mathrm{in}} = I_{\mathrm{in}} \cdot V_{\mathrm{in}}$, consisting of current I_{in} and voltage V_{in}, provided by the power supply. The solar cells cool down until an equilibrium is reached between input power and ambient conditions. The cooling procedure can be described by effects of conduction (q_{c}), convection (q_{cv}) and radiation (q_{rad}) as shown in equations (2), (3) and (4), respectively. All parameters are explained in Table 2.

$$q_c = \frac{k}{L} A (T_{\mathrm{cell}} - T_{\mathrm{env}}) \tag{2}$$

$$q_{\mathrm{cv}} = hA (T_{\mathrm{cell}} - T_{\mathrm{env}}) \tag{3}$$

$$q_{\mathrm{rad}} = \sigma A \left(\varepsilon T_{\mathrm{cell}}^4 - \alpha T_{\mathrm{env}}^4\right). \tag{4}$$

The energy lost due to conduction must be considered for each surface and material layer (encapsulation, glass and potentially backsheet) individually. Convection describes the energy emitted due to cooling on one surface. As the calculation performed will be compared to actual temperatures measured in the laboratory, the wind speed is considered 0 m/s on both sides. In outdoor application, convection needs to be adapted to wind speed and the PV module orientation towards it, as both impact the correct convection coefficient h [21]. Furthermore, in outdoor application it is possible that the ground heats up during the day and works as a heat source at night, which is neglected here for the indoor calculation at controlled temperatures. The energy emitted due to radiation is given by the Stefan-Boltzmann law of an object in a cooler environment.

As the energy is emitted on both sides of the cell equally (due to the shape of a solar cell, the heat distribution is simplified to be one dimensional), all described emission processes must be considered for both sides of the PV modules and their potentially different layers. Adapting Rim et al. [12], the whole energy balance can therefore be expressed as

$$\frac{T_{\mathrm{cell}} - T_{\mathrm{env}}}{2R_{\mathrm{c,EVA}} + R_{\mathrm{c,g}} + R_{\mathrm{c,bs}} + R_{\mathrm{cv,g}} + R_{\mathrm{cv,bs}}} + \sigma A \left(\varepsilon T_{\mathrm{cell}}^4 - \alpha T_{\mathrm{env}}^4\right) = I_{\mathrm{in}} V_{\mathrm{in}} \tag{5}$$

with the thermal resistance of conduction $R_{\mathrm{c},i} = L/k_i A$ for encapsulant, glass and backsheet (i = EVA, g, bs) and the thermal resistance of convection $R_{\mathrm{cv},j} = 1/hA$ for glass and backsheet (j = g, bs), respectively. Whereas, for the bifacial module both sides are equal as the backsheet is absent but replaced with an additional layer of glass. All parameters are explained and listed in Table 2. Solving equation (5) for T_{cell} gives the maximum temperature the cell reaches in equilibrium of supplied power versus ambient temperature.

2.4 Experimental setup

The experimental approach is conducted in a laboratory with the setup schematized in Figure 1. The ambient temperature was kept at 25 °C (±1 °C), monitored by an external thermometer placed one meter away from the module. The power to backpower the module is provided by a *TTi* power supply. The parameters (current, voltage, power) are measured by a *Fluke* multimeter. The module temperature is measured by a *Lutron* thermometer with T-thermocouples in four positions, as described in Table 1 and depicted in Figure 1. The thermocouples are placed on the PV module surfaces and attached with an aluminium adhesive tape. In front of the PV module, two cameras are placed; a *FLIR* IR camera to survey possible formation of hot spots and a *Raptor* camera with InGaAs sensor to capture the EL images. The power supply is started with the module specific current (I_{SC} and $0.1 \times I_{\mathrm{SC}}$, one after the other) and the voltage range is chosen with 30% above V_{OC} to ensure no current limitation. For the whole heating and cooling time, all data is logged. Further description of the equipment and the used time steps to record data can be found in Appendix A.

2.5 Dark *I–V* simulations

Like all PSUs, EL-ready inverters have a specific power window. As an example, the boundary values of an adapted *HUAWEI SUN2000-175KTL* are used. This prototype allows backpowering of connected PV strings with currents between 0 and 15 A and voltages between $V_{\mathrm{min}} = 1131$ V and $V_{\mathrm{max}} = 1500$ V. To estimate the EL functionality in terms of PV module string size and cell temperatures, a *MATLAB Simulink* model was developed, able to simulate the dark I–V curves of a PV module string. The model follows the example of [27] with the equation of the

Table 2. Description of used parameters for energy balance calculations in equation (5) to achieve saturation temperature of backpowered photovoltaic modules.

Symbol	Description	Unit	Value
T_{cell}	Solar cell temperature	K	
T_{env}	Ambient temperature	K	298.15
h	Convective coefficient	$\mathrm{W/m^2/K}$	6 (derived from [21] for no wind)
k_{EVA}, k_{g}, k_{bs}	Thermal conductivity of encapsulant, glass and backsheet	W/m/K	0.34 [22], 0.8 [23], 0.25 [24]
L_{EVA}	Encapsulant thickness	mm	0.45 [23]
L_{g}	Glass thickness	mm	2 (HJT), 3.2 (PERC + IBC)
L_{bs}	Backsheet thickness	mm	0.35
σ	Stefan-Boltzmann constant	$\mathrm{W/m^2/K^4}$	$5.67 \cdot 10^{-8}$
A	Solar cell area	$\mathrm{cm^2}$	243.7 (HJT + PERC), 150.0 (IBC)
ε_{g}	Emissivity of glass	–	0.9 [25]
$\varepsilon_{\mathrm{bs}}$	Emissivity of backsheet	–	0.83 [24]
α	Absorptivity of solar cell	–	0.93 [26]

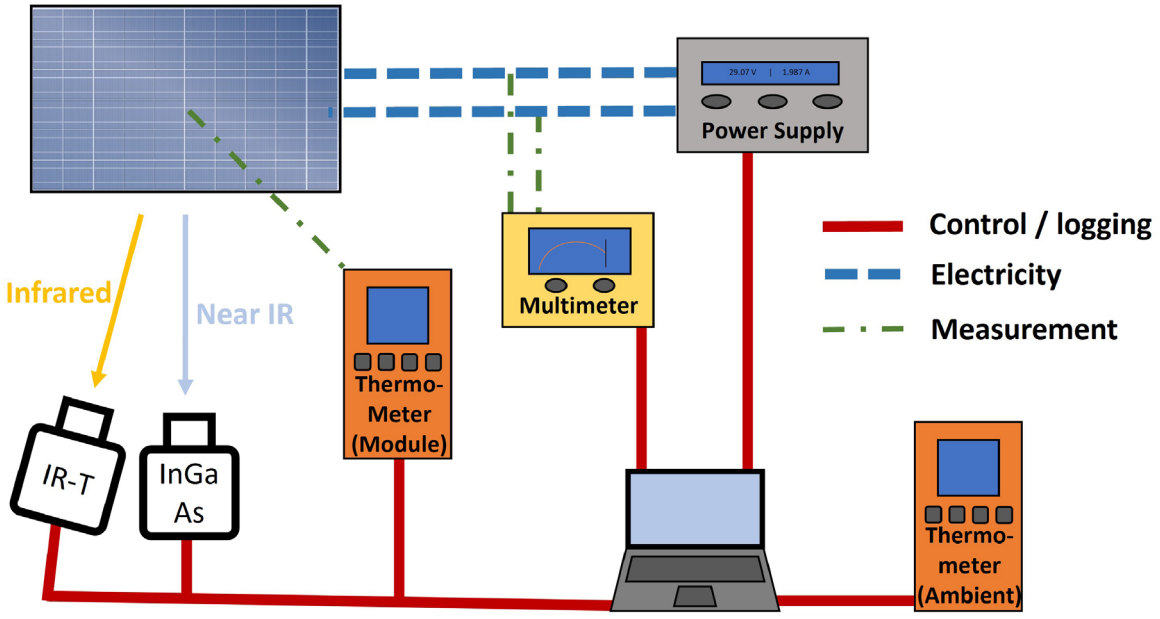

Fig. 1. Schematic of the experimental setup to survey the heating of a PV module during EL inspection.

one-diode model for strings of modules given by

$$I = I_{\mathrm{PV,cell}} \cdot N_{\mathrm{par}} - I_0 N_{\mathrm{par}} \left[\exp \frac{V + R_{\mathrm{S}} \mathrm{I} \frac{N_{\mathrm{ser}}}{N_{\mathrm{par}}}}{V_t \alpha N_{\mathrm{ser}}} - 1 \right] - \frac{V + R_{\mathrm{S}} I \frac{N_{\mathrm{ser}}}{N_{\mathrm{par}}}}{R_{\mathrm{SH}} N_{\mathrm{ser}}} \tag{6}$$

with $I_{\mathrm{PV,cell}}$ being the photovoltaic current, N_{par} and N_{ser} the number of parallel and in series connected PV modules, I_0 the saturation current, V the module voltage, R_{S} and R_{SH} series and shunt resistance, I the current, α the diode ideality constant and with the terminal voltage $V_{\mathrm{t}} = N_{\mathrm{s}} k_{\mathrm{B}} T_{\mathrm{cell}} / q$ with N_{s} number of cells in series in one PV module, k_{B} the Boltzmann constant, T_{cell} the cell temperature and q the elementary charge. The unknown parameters are extracted using the iterative method described in [27]. The simulation is then performed for a string of HJT modules and cell temperatures between −25 °C and +45 °C. The HJT module is a bifacial PV module. Analytic models for bifacial PV modules usually recognize the front and back side of the cell separately, resulting in $I_{\mathrm{PV,cell}} = I_{\mathrm{PV,front}} + I_{\mathrm{PV,rear}}$ with photovoltaic current due to irradiation on front ($I_{PV,\mathrm{front}}$) and rear side ($I_{\mathrm{PV,rear}}$) of the solar cell [11]. The double circuit model recognizes as well different loss parameters like difference

Table 3. Description of T-thermocouple positions as depicted in Figure 2.

Variable	Position description
T_1	Front above centered cell
T_2	Rear side above centered cell
T_3	Rear side in central cell gap
T_4	Rear side above corner cell

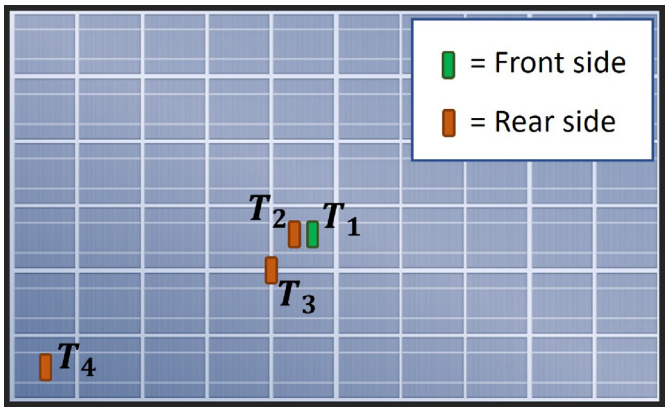

Fig. 2. Schematic showing the positions of the T-thermocouples to survey the module temperature. Including the used measurement point names, T_1 to T_4.

in resistances for both sides of the cell, while the double irradiance model considers only the two currents but concentrates the loss parameters. In this work, as only the dark I–V curves are of interest, the differentiation into two photovoltaic currents is neglected. To account for increased losses during backpowering, the voltage difference of V_{OC} to applied voltage, derived from experiments, is added to the voltage used for dark I–V simulations.

3 Results

3.1 Calculation

In Table 3, the cell saturation temperatures for the different modules calculated following equation (5) are given, as maximum temperature $T_{\mathrm{sat,calc}}$ and the over temperature as difference to the ambient temperature ($T_{\mathrm{amb}} = 25\,°\mathrm{C}$) as $\Delta T_{\mathrm{sat,calc}} = T_{\mathrm{sat,calc}} - T_{\mathrm{amb}}$. For all PV modules the increase in temperature is calculated to be between 20 °C (HJT) and 24.4 °C (IBC).

3.2 Experimental results

The measurements of $0.1 \times I_{\mathrm{SC}}$ resulted in temperature increases of below 2 °C. This alteration is too small to allow deeper inspections with the used setup. Therefore, all results and discussion are given for the I_{SC} inspection. From the measurements, several plots are depicted, shown exemplary for the HJT module in Figure 3. For a better overview, the corresponding plots for PERC and IBC modules are moved to Appendix B (Figs. B.1 and B.2, respectively). For each module, Subplot (a) shows the whole measurement cycle of each PV module, the supplied current, voltage and front-cell temperature as well as ambient temperature. A detailed inspection of the different measured module temperatures is given in Subplots (b), together with ambient temperature and the input voltage for a better orientation. Further, the results of the EL inspections are shown by the overall EL intensities of the module in Subplots (c). Finally, the normalized average EL intensity of a center cell and a corner cell of the same PV module are measured over the whole heating process and compared to each other in Subplots (d). Throughout this article, references to these subplots include the figures for all modules (Figs. 3, B.1 and B.2). No hot spots are present during the measurement, as confirmed by the IR-T images, of which an example image is shown for the HJT module in Figure 4.

The voltages at begin (V_{start}) and end (V_{end}) of backpowering are given, as well as their difference (ΔV). For the measured range, the temperature coefficient of the voltage compared to the front-cell temperature is calculated with an average of β_{V} with a standard deviation $\sigma_{\beta,\mathrm{dev}}$. To compare the heating velocity of the different technologies, the time until saturation temperature is reached (t_{heat}) is calculated, defined as the time from PSU start until the temperature is stable, meaning variation in the following 10 min is below 0.5 °C. Also, the cooling time (t_{cool}) is presented, defined as time from PSU-off until the module temperature is within 1 °C of the ambient temperature. The specific heating power $P_{\mathrm{EL,spec}}$ shows the power supplied during EL in relation to the active area of the PV module. All results are listed in Table 4.

The EL signal intensity is taken as average value of all pixels in the active module area. To account for camera internal variations during the measurement, e.g. due to sensor temperature changes, the average pixel value of the background area in each image is calculated as well and the EL signal intensity adapted to the resulting relative change. Further image editing was not performed to avoid quantitative alteration of the recorded signal. The intensity is normalized to the maximum value of each measurement cycle. Next to the plotted EL intensity in Sublopts (c), the total measured EL-intensity drop $\Delta\Phi_{\mathrm{EL}}$ is given in Table 4. The maximum difference between the measured EL intensities of a center and a corner cell are given by $\Delta\Phi_{\mathrm{EL,cells}}$.

3.3 The EL window

Following the difference between datasheet open circuit voltage and actually applied voltage, derived from the measurements, the dark I–V curves are simulated for a string of HJT modules with an open circuit voltage increased by 10%. The following parameters are derived: Series resistance $R_S = 0.447\Omega$, shunt resistance $R_{SH} = 444.6\Omega$ and dark saturation current at room temperature $I_0\,(298\mathrm{K}) = 2.85\,\mathrm{nA}$. The simulated dark I–V curves of a string consisting of 25 HJT modules are plotted for different temperatures in Figure 5.

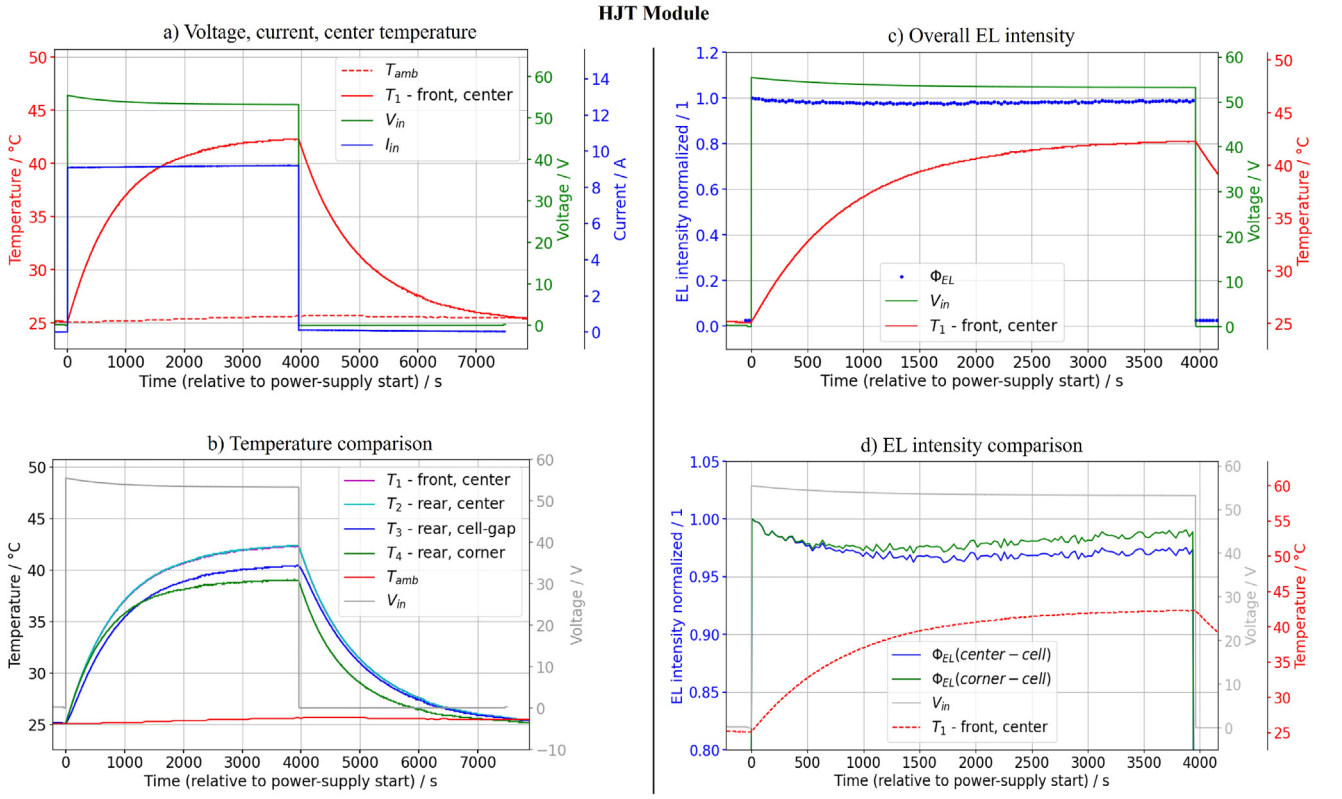

Fig. 3. Experimental results of HJT module. Voltage, current and centered cell temperature (a), comparison of all temperatures measured (b), evolution of the electroluminescence signal over measurement time (c) and comparison of two electroluminescence signals measured for a center and a corner cell of one module (d).

4 Discussion/conclusion

4.1 Temperatures

The results show a deviation between measurement and calculation. The calculated temperature ($T_{\mathrm{sat,calc}}$) is 3 °C (HJT) to about 5.5 °C (PERC, IBC) higher than the measured one ($T_{1,\mathrm{max}}$). The deviation can be explained by multiple reasons: the calculation was done to estimate the actual cell temperature, while the experiment did allow only measurement of the PV module surface temperatures. Further, the aluminium adhesive tape used to fix the thermocouples to the module surface does not isolate them completely from the ambient, resulting in the measured cell surface temperature being influenced by the ambient temperature. The difference in offsets between the various module technologies can be explained on one hand by the thinner front glass of the HJT module (2 mm compared to 3.2 mm for PERC and IBC), resulting in measured temperatures closer to the cell temperature. On the other hand, some material parameters (material emissivities and cell absorptivity), necessary for the calculation, are generalized for all modules investigated and possible technology-specific differences are not considered. In general, the IBC module experienced the strongest temperature increase, which can be explained by the higher specific heating power $P_{\mathrm{EL,spec}}$ compared to the other modules.

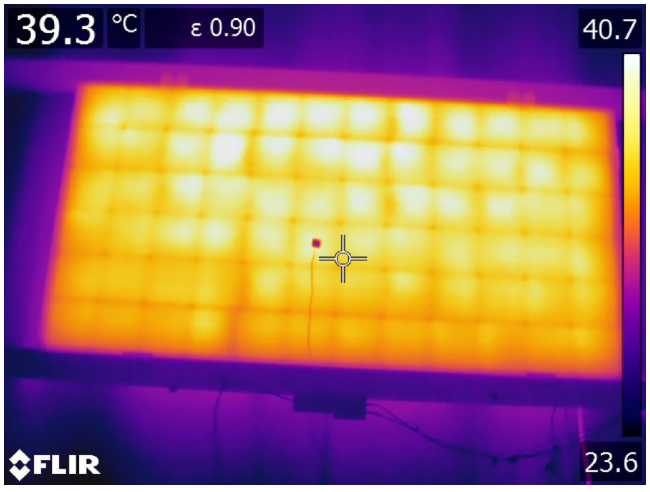

Fig. 4. Infrared thermography image of the HJT module under backpowering with short-circuit current. No formation of hot spots visible at the temperature measurement points.

The difference in conductive resistance of backsheet and glass can be seen by the temperature shown in Subplots (b), where the modules with common backsheets show a slightly higher temperature on the rear side (T_2) compared to the front (T_1), while the one of the bifacial HJT module (same glass layers on both sides) are not distinguishable.

Table 4. Results of the experimental measurements.

Symbol	Explanation	HJT	PERC	IBC	Unit
$T_{\mathrm{sat,calc}}$	From equation (5)	45.07	47.67	49.40	°C
$\Delta T_{\mathrm{sat,calc}}$		20.07	22.67	24.40	°C
$T_{1,\mathrm{max}}$	Front center cell	42.3	42.2	43.5	°C
$\Delta T_{1,\mathrm{max}}$		17.1	17.2	18.8	°C
$T_{2,\mathrm{max}}$	Rear center cell	42.4	42.4	43.7	°C
$\Delta T_{2,\mathrm{max}}$		17.2	17	18.6	°C
$T_{3,\mathrm{max}}$	Rear, cell gap	40.5	41.3	41.1	°C
$\Delta T_{3,\mathrm{max}}$		15.3	16	16.3	°C
$T_{4,\mathrm{max}}$	Rear, corner cell	39.1	39.5	39.1	°C
$\Delta T_{4,\mathrm{max}}$		14	14	14	°C
V_{start}	PSU on	55.49	42.56	67.44	V
V_{end}	PSU off	53.27	40.8	64.48	V
ΔV	$V_{\mathrm{start}} - V_{\mathrm{end}}$	−2.22	−1.76	−2.96	V
ΔV_{cell}	$\Delta V/\#\,cells$	−0.031	−0.029	−0.031	V
ΔV_{Voc}	$\Delta V/V_{\mathrm{OC}}$	−4.2	−4.4	−4.6	%
β_V	Average	−0.26	−0.27	−0.26	%/°C
$\sigma_{\beta,\mathrm{dev}}$	Standard deviation	±0.02	±0.016	±0.023	±%/°C
t_{heat}	Heating time	2576	1723	1740	s
t_{cool}	Cooling time	2674	1662	1709	s
$P_{\mathrm{EL,spec}}$	$\frac{V_{\mathrm{start}}\cdot I_{\mathrm{SC}}}{A_{\mathrm{cell}}\cdot N_{\mathrm{cell}}}$	266.8	264.0	301.8	W/m^4
$\Delta\Phi_{\mathrm{EL}}$	EL intensity drop	2	12	7	%
$\Delta\Phi_{\mathrm{EL,cells}}$	$\Delta\Phi_{\mathrm{EL,center}} - \Delta\Phi_{\mathrm{EL,corner}}$	−1.5	−4	−3	%

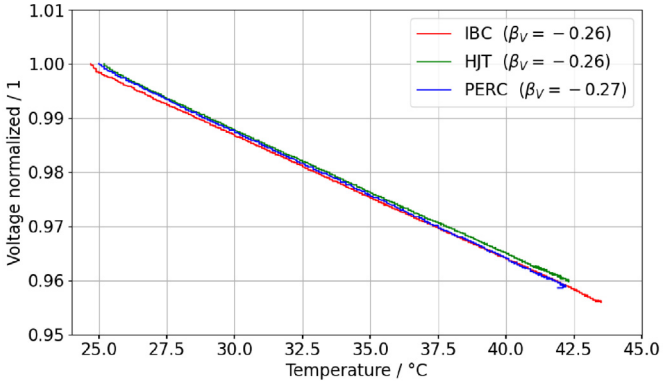

Fig. 5. Normalized voltage versus the temperature for all three modules investigated. Resulting β_{V} as average over the whole measurement with standard deviations given in Table 4.

The effects of lateral distribution of thermal energy through the modules can be seen in curves T_3 and T_4 of Subplots (b). Although the corner cell heats up as quickly as the center cell in the beginning, it is only partially surrounded by other cells and ends in a much cooler equilibrium compared to the center cells. The center cells instead are completely surrounded by other cells, thus heat sources, and therefore have less heat losses by lateral distribution. This results in a difference of corner compared to center cells of around 3 °C for HJT and PERC technology, while the difference is with 4.6 °C much stronger for the IBC module. An explanation for this can be the solar cell size, which is significantly smaller compared to the other modules, resulting in reduced cooling effects. T_3 in Sublots (b) visualizes the delay of lateral heat distribution, as it increases slowly in the beginning (longer distance to the actual heat source), but in the end results in a saturation temperature between the module temperatures measured above cells in the center and at the corner. The same effects can be seen in a reversed manner during the cooling process.

The parameters t_{heat} and t_{cool} show that heating and cooling of a module takes about the same time. PERC and IBC modules need about half an hour, and the HJT module around 43 min, to reach their saturation temperatures. Considering EL inspections performed by UAVs, the fly-over of single strings takes a few minutes maximum. Therefore, if the backpowering is planned precisely, the temperature increase of the modules will stay below half of the saturation temperature increase (about 10 min of backpowering). Ground-based inspection of one string can easily take 20 min, which is enough time for the modules to reach close to saturation temperature. It is advisable to maintain the backpowering time as short as possible, also to minimize the energy fed into the system.

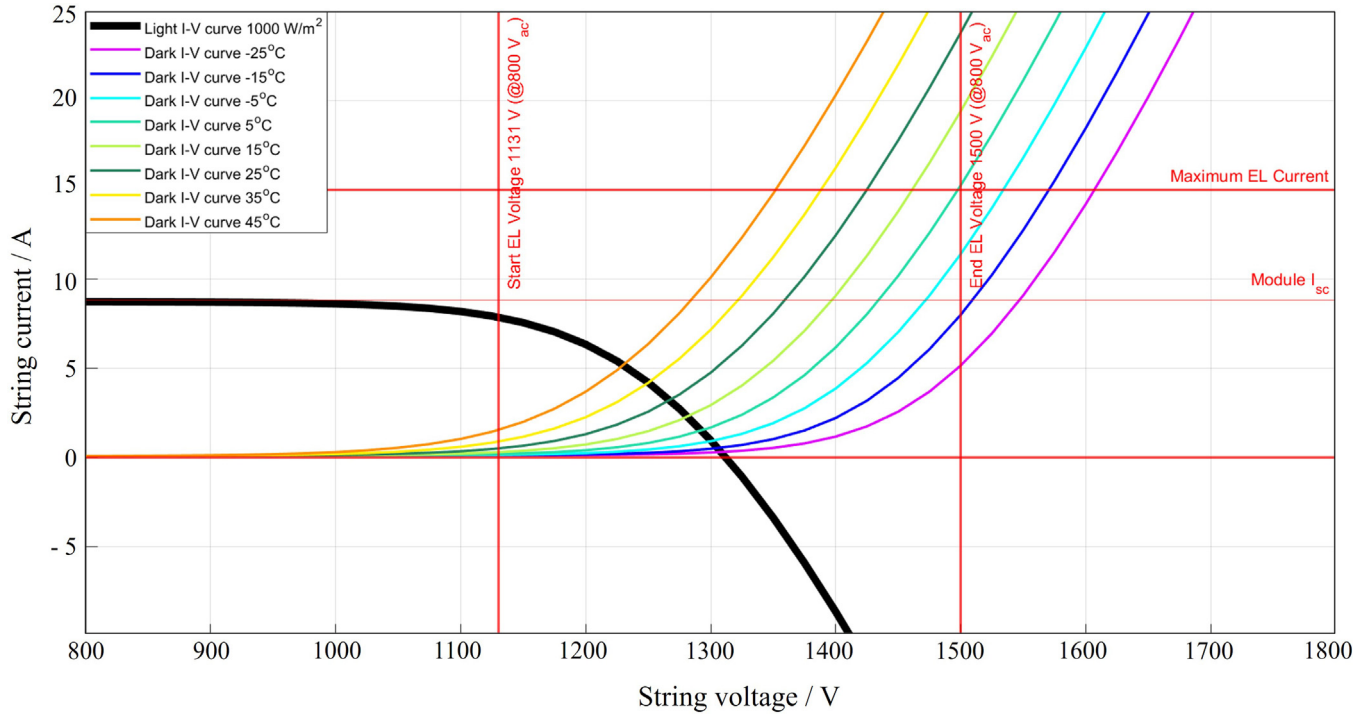

Fig. 6. *I–V* curves simulated for a string of 25 HJT modules in series. Light *I–V* at STC conditions (black thick line) and dark *I–V* curves simulated for temperatures between −25 °C and 45 °C. The red frame shows the EL window, in which the described *HUAWEI* EL-ready inverter is able to backpower.

4.2 Voltage

While the cell temperature follows a positive exponential decay, the module voltage (necessary to maintain supply of short circuit current) drops exponentially for all modules. The total voltage drop (ΔV) differs for the different modules. This is due to the number of cells and resulting V_{OC} of the modules. Taking this into account, the voltage drop per cell ΔV_{cell} is about −0.03 V for all module types. Figure 5 shows the normalized voltage in relation to the temperature. Throughout the whole investigated temperature range, this relation is linear for all modules, resulting in similar thermal voltage coefficients (β_V, cf. Tab. 4) around −0.26 °C. They are comparable to the respective data sheets thermal coefficients for V_{OC} ($\beta_{V_{oc}}$, cf. Tab. 1) with deviations between 0% (IBC) and 13% (PERC).

4.3 EL intensity

The EL intensity behaviour shown in Subplots (c) follows roughly the applied voltage. While the PERC module shows a strong decrease of 12% in measured EL intensity, it is almost constant with only 2% drop for the HJT module. The progression of the measured EL intensity is not strictly continuous and covered by noise, which can be seen especially for the IBC and the HJT module (Figs. B.2c and 3c, respectively). Different cell technologies can have an impact on the intensity drop and therefore might have a an effect on the variation in $\Delta\Phi_{EL}$. The noise within one measurement instead must come from the imaging procedure and not yet considered impact factors. Because this investigation is not in the scope of the present work, these results only show the trend of the temperature and voltage dependency of the EL signal intensity and can not be taken as definite numbers.

Nevertheless, the trend of EL signal intensity following the cell temperature can also be demonstrated within a single module, by comparing the measured intensities of a cell in the center with a corner one. The intensity developments over time of both cells, each normalized to one, can be seen in Subplots (d), which also allows a better observation of the aforementioned noise and inconsistency in the measured EL signal intensity. Comparing the two cells, the corner cell shows a slightly lower EL intensity variation of 1.5 (HJT) to 4 (PERC) percentage points and therefore maintains a stronger signal compared to the center cell.

4.4 The EL window

The EL window shows, for a certain setup, the possibility of performing EL inspections. The dark *I–V* curves of a given module string constellation (here 25 HJT modules, cf. Fig. 6) allow the estimation of best temperatures to perform EL inspection. Although the voltage range of the inverter is quite large, one sees immediately, that EL inspection with a current supply of I_{SC} is not possible for lower temperatures. The results of this simulation show that, in the presented case, low module temperatures (below −10 °C) prevent applying I_{SC}. Instead, high temperatures (above 40 °C) might cause problems with applying $0.1 \times I_{SC}$. While in the first case, the heating of the

modules during EL inspection can influence the measurement positively by shifting it inside the EL window (slow increase of current), in the second case, heating has a negative impact on maintaining the EL window.

Considering the temperature dependency of the voltage needed to supply I_{SC} with the voltage drop of $\Delta V = -2.2\,V$ per HJT module as described above, it results in a voltage drop of 55 V for the string of 25 HJT modules. Therefore, heating can shift the measurement voltage during EL significantly, and thus it must be considered to remain inside the EL window.

4.5 Snow melting possibility

Next to the EL inspections, the heating effect can have an added value if used for dealing with snow cower and loads on PV modules. Snow can be of advantage, especially for bifacial PV modules, if it covers the ground and therefore increases albedo from usually 10–30% up to 67–74% of the incident radiation [28]. But if the PV modules are covered by snow, they experience a significant reduction in power production due to decreased irradiance reaching the solar cells [29]. Furthermore, heavy snow loads and the accompanying moisture can result in increased degradation of PV modules. Melting snow by backpowering the modules is not a new approach, there are market-ready solutions using external power electronics to fulfil this task [30,31]. However, the additional setup needed makes it a costly procedure. If backpowering is available in already installed inverters, under consideration of the weather forecast, snow melting can become an economically feasible procedure. As an example calculation, a day of snow but with sunny days afterwards is considered, with ambient temperatures between 0 °C and −5 °C and a string of 25 HJT modules. If nothing is done and a snow layer builds up on the modules, the generated current will depend mainly on the albedo. Instead, applying $0.5 \times I_{SC}$ to the modules increases the module surface temperature by about $7 - 8$ °C (10.3 °C cell temeperature increase, calculated with ambient temperature of −3 °C and 1 m/s wind speed). To maintain this status, about 6 kW per hour (25 modules × 235 W) is needed. Depending on snow load and snowing time, the additional energy to melt the snow must be considered, and, by involving the weather forecast, estimated, if the additional energy produced in the following days pays back the one used for heating.

5 Summary and outlook

In this paper, the heating effect of backpowering PV modules during EL inspections is investigated theoretically and experimentally. An energy balance calculation allows to estimate the saturation cell temperatures of different PV technologies (HJT, PERC and IBC) under a forward current of I_{SC}. Measurements of the module surface temperatures at different positions during long-term backpowering allows to compare the calculated cell temperature with measured surface temperatures for all module technologies. For all investigated modules, the temperature increase is in the range of 20 °C. Measurement of the heating time shows that the heating plays a minor role for fast EL imaging by use of UAVs. Nevertheless, the resulting voltage drop due to temperature can reduce the string voltage by as much as the voltage of one whole PV module, as the example of a HJT module string shows. Therefore, planning of a PV plant with EL-ready inverters must be done carefully to ensure the voltage ranges of the inverters are not exceeded. To do so, the possible power ranges of an EL-ready inverter are presented as *EL window* in comparison to the simulated dark *I*–*V* curves of an HJT module string at different temperatures.

The applicability of the described heating effect to remove snow loads is discussed. If this is financially beneficial, depends on the weather conditions in the days after the snow is melted. A detailed trade-off analysis by combination of weather forecast, yield estimations and accurate melting power calculations for different snow cover levels are planned for future work. For a correct calculation in the field, the ground must be included as possible heat source, which can influence the PV module temperatures by thermal radiation.

For EL inspections, a drop in measured EL signal intensity due to the backpowering induced heating can be observed for all investigated cell technologies. The resulting numbers vary between 2% and 12%, but at the current state, due to an inconsistency in the measured EL signal intensity, these measurements only show the trend of EL signal intensity in following temperature and voltage. To calculate definite numbers, all impact factors on the intensity measurement must be identified and investigated in future work. Although the generated EL signal is already small, the approximately detected decline in intensity makes no practical difference for qualitative analyses done in outdoor conditions. The same is the case for the variation in EL intensity between center and corner cell through one module. But both described phenomena should be considered for quantitative EL measurements in laboratory conditions.

For future work, next to a detailed EL signal quantification, the usage of EL-ready inverters will be tested in a real-life application. Although still a prototype, if its functionality is proven and it becomes a standard in future PV installations, it will make EL inspections much faster. The time saved due to the avoidance of the requirement of using time intensive PSU installations will be a game changer as it can drive the outstanding detection possibilities of EL also financially in the range of IR-T inspections.

Funding

This work has received funding from the Horizon 2020 programme of the European Union under GA. No. 952957–Project TRUST PV.

Author contribution statement

L. Koester: Conceptualization, methodology, formal analysis, investigation, experimental, writing – original draft preparation, writing – review and editing, visualization. E. Vallarella: Formal analysis. A. Louwen: Writing – review and editing. S. Lindig: Writing – review and editing. D. Moser: Writing – review and editing, supervision.

Appendix A

Table A.1. Specification of equipment and time stamps used for measurements performed as described in Section 2.

Description	Model	Measured data / Resolution / Accuracy	Time steps
Power supply	TTi *QPX600DP*	–	–
Multimeter	FLUKE *435 Series II* + Current Clamp *i30s*	Voltage / 0.01 V / +- 0.1% Current / 0.001 A / +- 1%	0.25 s
Ambient temperature	E+E Elektronik *Humlog 20*	Temperature / 0.1 °C / ±0.3 °C	60 s
Cell Temperature	Lutron *TM-947SD* (4 x *T*-thermocouples)	Temperature / 0.1 °C / ±(0.4%+0.5 °C)	1 s
Hot Spots	FLIR *T630SC*	Thermographic image	15 s
EL	Raptor *OWL640mini*	Electroluminescence image	15 s

Appendix B

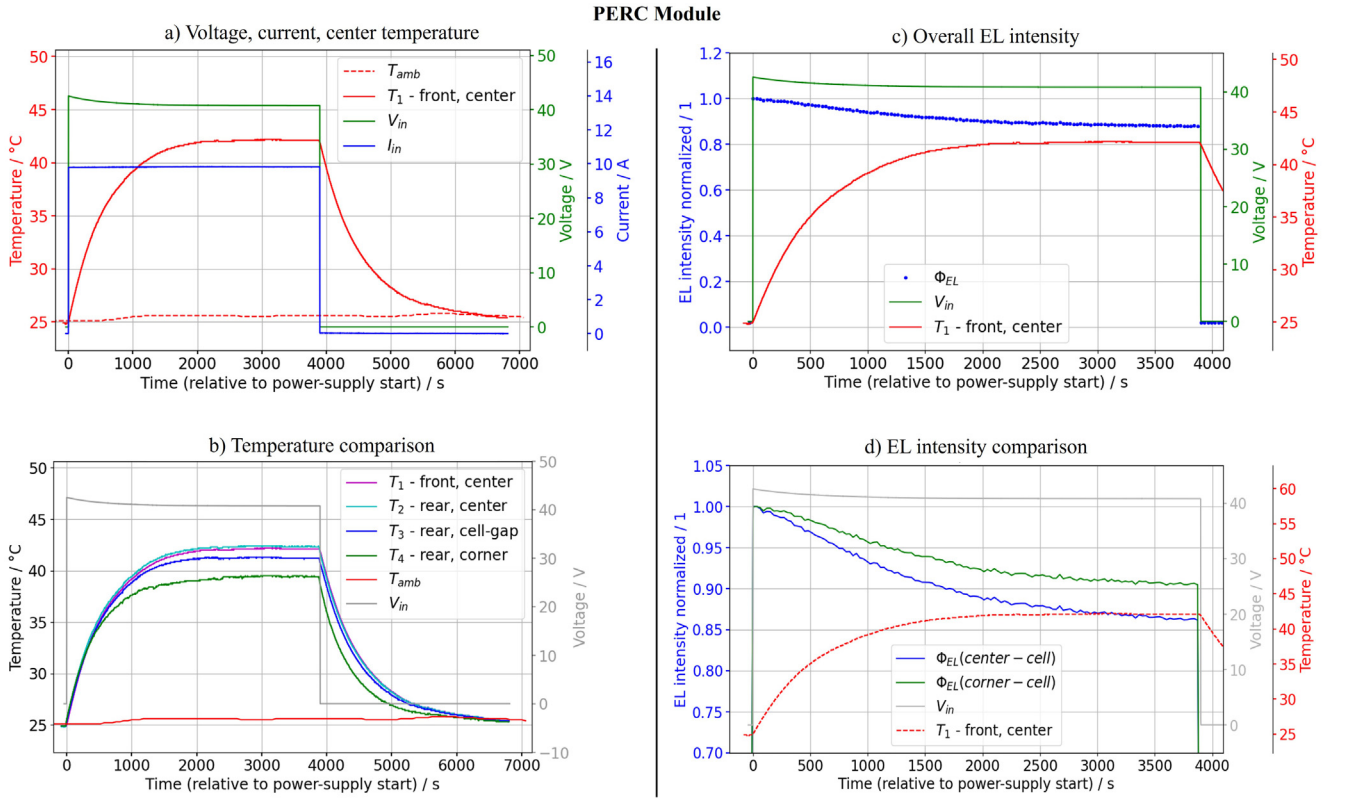

Fig. B.1. Experimental results of PERC module. Voltage, current and centered cell temperature (a), comparison of all temperatures measured (b), evolution of the electroluminescence signal over measurement time (c) and comparison of two electroluminescence signals measured for a center and a corner cell of one module (d).

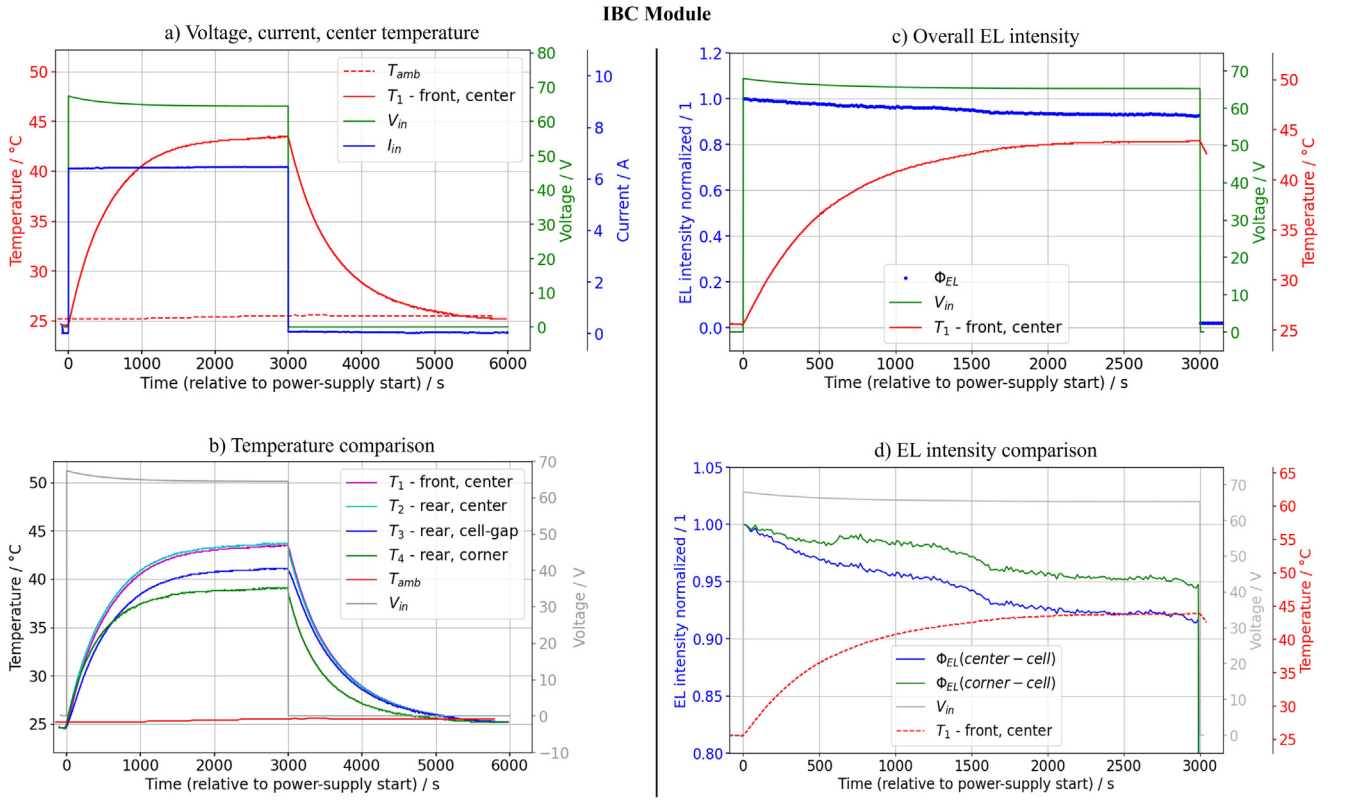

Fig. B.2. Experimental results of IBC module. Voltage, current and centered cell temperature (a), comparison of all temperatures measured (b), evolution of the electroluminescence signal over measurement time (c) and comparison of two electroluminescence signals measured for a center and a corner cell of one module (d).

References

1. IEC TS 60904-13, *Photovoltaic devices – part 13: Electroluminescence of photovoltaic modules* (Standard, International Electrotechnical Commission (IEC), Geneva, CH, 2018)
2. D. Kiliani, *Luminescence Imaging Techniques for Silicon Photovoltaics*, PhD thesis, University of Konstanz (2013)
3. W. Herrmann, G. Eder, B. Farnung, G. Friesen, M. Köntges, B. Kubicek, O. Kunz, H. Liu, D. Parlevliet, I. Tsanakas, J. Vedde, IEA-PVPS task 13: Performance, operation and reliability of photovoltaic systems – qualification of photovoltaic (PV) power plants using mobile test equipment. Report, International Energy Agency (2021)
4. IEC TS 62446-4, Photovoltaic (pv) systems – requirements for testing, documentation and maintenance - part 4: Electroluminescence measurement of photovoltaic arrays. electroluminescence of photovoltaic modules (Standard, International Electrotechnical Commission (IEC), Geneva, CH, Under Development)
5. S. Koch, T. Weber, C. Sobottka, A. Fladung, P. Clemens, J. Berghold, Outdoor electroluminescence imaging of crystalline photovoltaic modules: Comparative study between manual ground-level inspections and drone-based aerial surveys, in *32nd EUPVSEC* (2016), pp. 1736–1740
6. J. Ballestín-Fuertes, J. Muñoz-Cruzado-Alba, J.F. Sanz-Osorio, L. Hernández-Callejo, V. Alonso-Gómez, J.I. Morales-Aragones, S. Gallardo-Saavedra, O. Martínez-Sacristan, A. Moretón-Fernández, Novel utility-scale photovoltaic plant electroluminescence maintenance technique by means of bidirectional power inverter controller, Appl. Sci. **100**, 2076 (2020)
7. A. Louwen, A.C. de Waal, R.E.I. Schropp, A.P.C. Faaij, W.G.J.H.M. van Sark, Comprehensive characterisation and analysis of pv module performance under real operating conditions, Progr. Photovolt.: Res. Appl. **250**, 218 (2017)
8. S. Lindig, A. Louwen, D. Moser, M. Topic, Outdoor pv system monitoring—input data quality, data imputation and filtering approaches, Energies **13**, 5099 (2020)
9. S. Bouchakour, D.V. Caballero, A. Luna, E. Roman Medina, K.B. El Amin, P.R. Cortés, Monitoring, modelling and simulation of bifacial pv modules over normal and high albedos, in *2020 9th International Conference on Renewable Energy Research and Application (ICRERA)* (2020), pp. 252–256
10. G.M. Tina, F.B. Scavo, A. Gagliano, Multilayer thermal model for evaluating the performances of monofacial and bifacial photovoltaic modules, IEEE J. Photovolt. **100**, 1035 (2020)
11. B.G. Bhang, W. Lee, G.G. Kim, J.H. Choi, S.Y. Park, H.-K. Ahn, Power performance of bifacial c-si PV modules with different shading ratios, IEEE J. Photovolt. **90**, 1413 (2019)

12. S. Rim, M. Baldrias, M. Morse, Temperature of solar cells in reverse bias: Theory and applications, in *2010 35th IEEE Photovoltaic Specialists Conference* (IEEE, 2010), pp. 002698–002700
13. H.J. Solheim, H.G. Fjær, E.A. Sørheim, S.E. Foss, Measurement and simulation of hot spots in solar cells, Energy Procedia **38**, 183 (2013)
14. U. Rau, Reciprocity relation between photovoltaic quantum efficiency and electroluminescent emission of solar cells, Phys. Rev. B **76**, 085303 (2007)
15. L. Koester, A. Astigarraga, S. Lindig, D. Moser, Development of daylight photoluminescence technique for photovoltaic modules and investigation of temperature dependency, in *37th EU-PVSEC* (2020), pp. 908–913
16. L. Koester, E. Vallarella, A. Louwen, S. Lindig, D. Moser, WCPEC-8 proceedings (2022), pp. 1112–1118
17. E. Skoplaki, J.A. Palyvos, On the temperature dependence of photovoltaic module electrical performance: a review of efficiency/power correlations, Sol. Energy **830**, 614 (2009)
18. T. Ghanbari, Permanent partial shading detection for protection of photovoltaic panels against hot spotting, IET Renew. Power Gener. **110**, 123 (2017)
19. T. Fuyuki, H. Kondo, Y. Kaji, A. Ogane, Y. Takahashi, Analytic findings in the electroluminescence characterization of crystalline silicon solar cells, J. Appl. Phys. **1010**, 023711 (2007)
20. ITRPVl International Technology Roadmap for Photovoltaic (ITRPV), 12th edition. Technical report (VDMA Photovoltaic Equipment, Frankfurt am Main, Germany, 2021)
21. C. Schwingshackl, M. Petitta, J.E. Wagner, G. Belluardo, D. Moser, M. Castelli, M. Zebisch, A. Tetzlaff, Wind effect on PV module temperature: analysis of different techniques for an accurate estimation, Energy Procedia **40**, 77 (2013)
22. Makeitfrom database, https://www.makeitfrom.com/material-properties/10-Percent-Vinyl-Acetate-EVA (accessed: 08.07.2022)
23. A. Pfreundt, A.J. Beinert, D. Yucebas, L.V. Mesquita, L. Pitta-Bauermann, M. Mittag, Post-processing thickness variation of PV module materials and its impact on temperature, mechanical stress and power, in *36th EU-PVSEC* (2019)
24. J. Oh, B. Rammohan, A. Pavgi, S. Tatapudi, G. Tamizhmani, G. Kelly, M. Bolen, Reduction of PV module temperature using thermally conductive backsheets, IEEE J. Photovolt. **80l**, 1160 (2018)
25. A. Riverola, A. Mellor, D. Alonso Alvarez, L. Ferre Llin, I. Guarracino, C.N. Markides, D.J. Paul, D. Chemisana, N. Ekins-Daukes, Mid-infrared emissivity of crystalline silicon solar cells, Sol. Energy Mater. Sol. Cells **174**, 607 (2018)
26. R. Santbergen, R.J.C. van Zolingen, The absorption factor of crystalline silicon PV cells: A numerical and experimental study, Sol. Energy Mater. Sol. Cells **920**, 432 (2008)
27. M. Villalva, J. Gazoli, E. Filho, Modeling and circuit-based simulation of photovoltaic arrays, in *2009 Brazilian Power Electronics Conference, COBEP2009*, Vol. 14, pp. 1244–1254
28. S.N. Williamson, L. Copland, D.S. Hik, The accuracy of satellite-derived albedo for northern alpine and glaciated land covers, Polar Sci. **100**, 262 (2016)
29. M. Ali Anadol, E. Erhan. The effect of snowfall and icing on the sustainability of the power output of a grid-connected photovoltaic system in Konya, Turkey. Turk. J. Electr. Eng. Comput. Sci. **270**, 4608 (2019)
30. Eulektra solar reverter, https://www.eulektra.de/photovoltaik/hain-system/eulektra-solar-reverter/. Accessed: 07.07.2022
31. Innos weight watcher, https://www.innos.no/weight-watcher/. Accessed: 07.07.2022

Cite this article as: Lukas Koester, Emanuel Vallarella, Atse Louwen, Sascha Lindig, David Moser, Evaluating the effects of photovoltaic module heating during electroluminescence inspection, EPJ Photovoltaics **14**, 14 (2023)